

Eddy Current Tomography for Metal Solidification Imaging

Minh H. Pham^{*}, Yingbo Hua^{*}, Neil B. Gray^{**}

^{*}Department of Electrical and Electronic Engineering,
The University of Melbourne, Parkville, Victoria 3052 Australia,
E-mail: yhua@ee.mu.oz.au

^{**}G. K. William Co-operative Research Centre for Extractive Metallurgy,
Department of Chemical Engineering,
The University of Melbourne, Parkville, Victoria 3052 Australia

Abstract – *This paper presents a theoretical framework of imaging the solidification of molten metal inside a pipe by eddy currents. A complete mathematical model is developed which reveals the relationship between the solidification inside the pipe and the scattered field measurable outside the pipe. This model is then exploited to develop a numerical algorithm which is able to quickly reconstruct the geometry of the solidification based on the measured scattered field intensity. This framework not only appears to be the first of its kind from the metallurgical point of view, but also involves some novel development from the point of view of electromagnetic computations, which includes in particular the Green functions in multiple layered media.*

Keywords: eddy current tomography, electromagnetic field, numerical computation, solidification

1. INTRODUCTION

Electronic control system of molten metal flow is currently researched at two Australian Co-operation Research Centres. Monitoring the extent of solidification of molten metal flowing in a pipe is essential for controlling the flow. It has been proposed to use partial solidification of the fluid to control the flow rate [1]. As the melt solidifies, it generally forms a non-symmetrical layer of solidification which has a different conductivity from the melt. It is desirable to find the shape and the thickness of this layer by examining the conductivity distribution inside the pipe.

There appears no approach applicable for this imaging task other than that of eddy currents. Eddy-currents technique is a unique, nondestructive method for determining the conductivity of metals. It employs low frequency magnetic fields which penetrate into metals and create the so-called eddy currents. Eddy currents have a reasonable sensitivity to continuous and discontinuous changes in metals. Applications of eddy currents in casting of molten metal can be found in [2,3] and the more recent work [4]. To our knowledge, applying eddy currents for imaging metal solidification has not been reported before in literature except the one dimensional case [2].

This paper is organised as follows. Section 2 gives a general description of the problem, and section 3 formulates the problem quantitatively by partial differential equations. These partial differential equations are then transformed into integral equations using Green functions technique. A mathematical relationship between the scattered field seen from a solenoid and the metal solidification distribution is given through the set of integral equations. The electric field inside the pipe which is governed by one of the integral equations is solved using the moments method as shown in section 4. In section 5, an iterative algorithm for reconstructing the solidification distribution using a perturbation technique is described. The iterative algorithm requires the computation of electric field inside the pipe at each iteration. Section 6 suggests a procedure to speed up this process. Section 7 provides the simulation results to support our theory.

2. DESCRIPTION OF THE PROBLEM

The geometry of the problem is shown in Figure 1. There are two types of media considered here, namely air and conductor. The cylindrical pipe containing molten metal is penetrated with a time-varying magnetic field from a solenoid. This field creates eddy currents circulating in the conductor. The pattern of the currents depends on the conductivity distribution.

The eddy currents in turn produce a scattered field which can be sensed in the region exterior to the pipe. Based on the external measurements, the shape and the thickness of solidification can be determined.

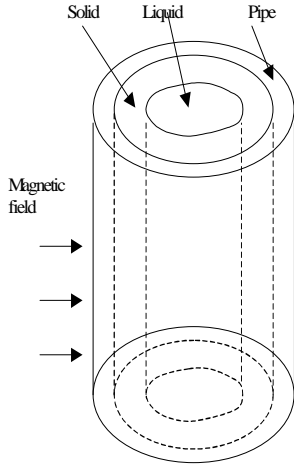


Figure 1: Pipe penetrated by magnetic field

We will assume that the cylindrical pipe under consideration is penetrated with a transverse magnetic (TM) field. This TM field can be generated by a long rectangular solenoid where the end effect is neglected. Since the solidification is assumed to be invariant in the z -direction, the dominating field is approximately z -invariant. The problem is hence reduced to a two-dimensional one. The TM field consists of two components: angular component and radial component. It is assumed that the media are linear and the excitation is at a single (radian) frequency ω .

3. MODELLING

3.1 Conductivity profile modelling

We divide the whole space under consideration into three regions (as shown in Figure 2): Region I (Ω_1) is the space inside the pipe; Region II (Ω_2) is the pipe; and Region III (Ω_3) is the air outside the pipe.

In our problem, the electric field consists of only one component in the z -direction. The electric field in Region I (circle of radius r_1) is governed by (assuming $\omega \ll s_1$) [5]:

$$\nabla^2 E_1(\mathbf{r}) - j\omega s_1(\mathbf{r}) E_1(\mathbf{r}) = 0 \quad (1)$$

where $\mathbf{r} = (r, j)$ is the position vector in cylindrical coordinate, ∇^2 the Laplacian operator, μ permeability, ϵ permittivity, $s_1(\mathbf{r})$ conductivity distribution in region I and is a function of position.

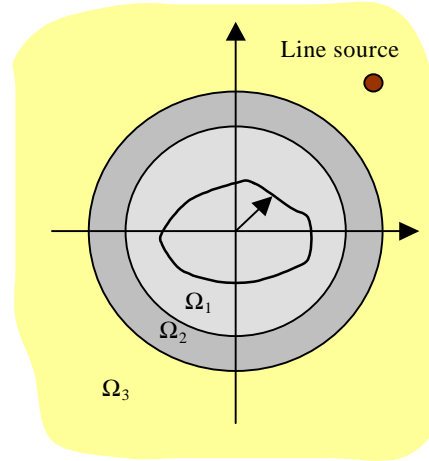


Figure 2: Cross section (Region I Ω_1 , Region II Ω_2 , Region III Ω_3)

In region I, the molten metal is surrounded by a layer of solidification of arbitrary shape. We model the boundary between the melt and the solid by a function $0 \leq r(j) \leq r_1$, $0 \leq j \leq 2\pi$. In general, there is also a mushy zone, where solid and liquid phases co-exist. A microscopic investigation of this zone has been carried out by many [6,7]. We however only consider the macroscopic property of the mushy region by assuming that the conductivity is smoothly distributed in the mushy region.

A model of the conductivity distribution $s_1(\mathbf{r})$ is given below:

$$s_1(\mathbf{r}) = s_s \left(1 - \frac{s_s - s_l}{s_s} f(\mathbf{r}) \right) \quad (2)$$

where s_s is the conductivity of the solidified metal; s_l is the conductivity of molten metal; $f(\mathbf{r})$ is defined as:

$$f(\mathbf{r}) = \frac{1}{2} - \frac{\tan^{-1}\{a[r - r(j)]\}}{\pi} \quad (3)$$

which is a monotonic function of r . The parameter a determines the thickness of the mushy zone. Figure 3 shows an example of f . It should be kept in mind that $f(\mathbf{r})$ depends on the shape function $r(j)$ and the parameter a . Since the conductivity distribution $s_1(\mathbf{r})$ is proportional to $f(\mathbf{r})$, we will use the name distribution or profile for both. Note that as a approaches ∞ , the mushy zone disappears since f approaches a step function:

$$f(\mathbf{r}) = \begin{cases} 1, & r < r(j) \\ 0, & r > r(j) \end{cases} \quad (4)$$

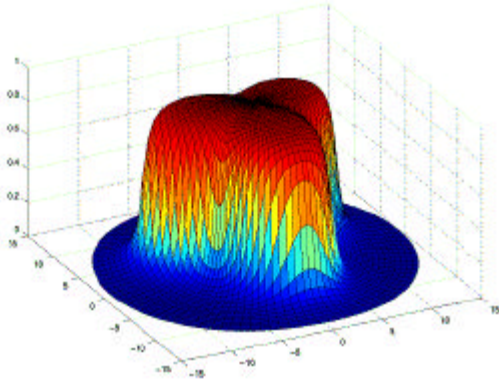


Figure 3: Mushy zone between liquid and solid where $r(j)=8+2\sin(3j)$ and $a=2.0$

Denote $j\omega\mathbf{s}_{-s}$ by k_1^2 , the equation (1) is rewritten as:

$$\nabla^2 E_1(\mathbf{r}) - k_1^2 E_1(\mathbf{r}) = -k_1^2 \frac{\mathbf{s}_s - \mathbf{s}_l}{\mathbf{s}_s} f(\mathbf{r}) E_1(\mathbf{r}) \quad (5)$$

The term on the RHS of (5) represents the change of eddy current distribution with respect to the background conductivity \mathbf{s}_s . The electric fields in the remaining regions II and III (pipe and air) are:

$$\nabla^2 E_2(\mathbf{r}) - k_2^2 E_2(\mathbf{r}) = 0, \quad k_2^2 = j\omega\mathbf{s}_2 \quad (6)$$

$$\nabla^2 E_3(\mathbf{r}) - k_3^2 E_3(\mathbf{r}) = j\omega\mathbf{J}(\mathbf{r}), \quad k_3^2 = -\omega^2 \mu \epsilon \quad (7)$$

where \mathbf{s}_2 is the conductivity of the pipe, and $\mathbf{J}(r, \mathbf{j})$ the current source in the air region. In eddy currents problems, the frequency ω is small and the constant k_3 is negligible (often set to zero). Equations (5), (6) and (7) together with proper boundary conditions [5] completely describe the behaviour of the electromagnetic fields in our setting.

3.2 Relationship Between Conductivity Profile and Scattered Field

Considering (5) to (7), we define the Green function G_u^v for region u due to a delta source in region v as follows:

$$\nabla^2 G_u^v(\mathbf{r}, \mathbf{r}') - k_u^2 G_u^v(\mathbf{r}, \mathbf{r}') = \mathbf{d}_u^v \delta(\mathbf{r} - \mathbf{r}') \quad (8)$$

where $\mathbf{d}_u^v = 1$ if $u = v$ and 0 otherwise. All boundary conditions must also be satisfied by G_u^v . It follows from a superposition theorem [8] that:

$$E_1(\mathbf{r}) = -j\omega\mu \int_{\Omega_3} G_1^3(\mathbf{r}, \mathbf{r}') J(\mathbf{r}') d\Omega' + I \int_{\Omega_1} G_1^1(\mathbf{r}, \mathbf{r}') f(\mathbf{r}') E_1(\mathbf{r}') d\Omega' \quad (9)$$

$$E_3(\mathbf{r}) = -j\omega\mu \int_{\Omega_3} G_3^3(\mathbf{r}, \mathbf{r}') J(\mathbf{r}') d\Omega' + I \int_{\Omega_1} G_3^1(\mathbf{r}, \mathbf{r}') f(\mathbf{r}') E_1(\mathbf{r}') d\Omega' \quad (10)$$

where $I = k_1^2(\mathbf{s}_s - \mathbf{s}_l)/\mathbf{s}_s$. The electric field $E_2(\mathbf{r})$ in region II is of no interest to us. The first integral in each of (9) and (10) represents the contribution from the applied current source. When the current source of magnitude I_0 is carried by a very long and thin solenoid, it is convenient to model it as a delta function:

$$\mathbf{J}(\mathbf{r}) = I_0 \mathbf{d}(\mathbf{r} - \bar{\mathbf{r}}) \quad (11)$$

where $\bar{\mathbf{r}}$ is the position of the source. It follows that:

$$E_1(\mathbf{r}, \bar{\mathbf{r}}) = E_{i1}(\mathbf{r}, \bar{\mathbf{r}}) + I \int_{\Omega_1} G_1^1(\mathbf{r}, \mathbf{r}') f(\mathbf{r}') E_1(\mathbf{r}', \bar{\mathbf{r}}) d\Omega' \quad (12)$$

$$E_3(\mathbf{r}, \bar{\mathbf{r}}) = E_{i3}(\mathbf{r}, \bar{\mathbf{r}}) + I \int_{\Omega_1} G_3^1(\mathbf{r}, \mathbf{r}') f(\mathbf{r}') E_1(\mathbf{r}', \bar{\mathbf{r}}) d\Omega' \quad (13)$$

The first term of (12) and (13) are given by:

$$E_{i1}(\mathbf{r}, \bar{\mathbf{r}}) = -j\omega I_0 G_1^3(\mathbf{r}, \bar{\mathbf{r}}) \quad (14)$$

$$E_{i3}(\mathbf{r}, \bar{\mathbf{r}}) = -j\omega I_0 G_3^3(\mathbf{r}, \bar{\mathbf{r}}) \quad (15)$$

They are incident fields due to the external source.

Once these equations for a particular line source configuration are solved, the fields due to an arbitrary shape of solenoid can be easily obtained by superposition. We define the scattered field measured in the solenoid as:

$$E_s(\mathbf{r}, \bar{\mathbf{r}}) = E_3(\mathbf{r}, \bar{\mathbf{r}}) - E_{i3}(\mathbf{r}, \bar{\mathbf{r}}) \quad (16)$$

Then it can be written as:

$$E_s(\bar{\mathbf{r}}) = I \int_{\Omega_1} G_3^1(\bar{\mathbf{r}}, \mathbf{r}') f(\mathbf{r}') E_1(\mathbf{r}', \bar{\mathbf{r}}) d\Omega' \quad (17)$$

The equation (12) together with (15) define the relationship between the distribution (represented by $f(\mathbf{r})$) and the observable scattered field.

4. SOLUTION OF ELECTRIC FIELD BY MOMENTS METHOD

The total electric field $E_1(\mathbf{r}, \bar{\mathbf{r}})$ governed by (12) is solved using the moments method [9,10]. We provide numerical results for the case when the basis functions are polynomials and sinusoids; the solid-liquid interface is circular and no mushy zone presented. This is a good example to see how well the numerical results agree with the analytical solution.

Figure 4 and 5 show the real and imaginary part of the electric field. Figure 6 and 7 show the percentage error compared to the analytical solution [8] is less than 0.05 %.

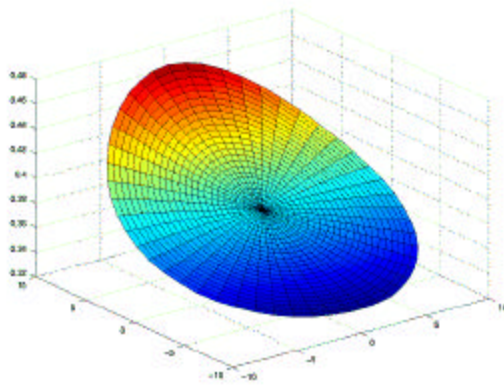


Figure 4: Electric field (Real) for circular domain

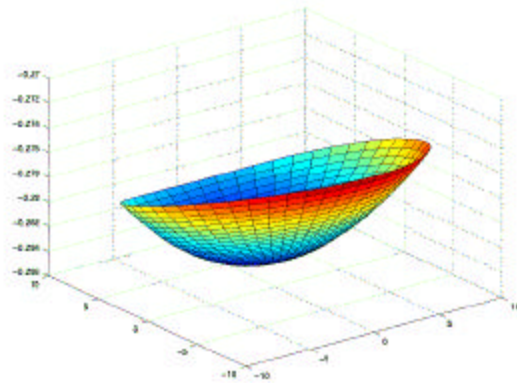


Figure 5: Electric field (Imaginary) for circular domain

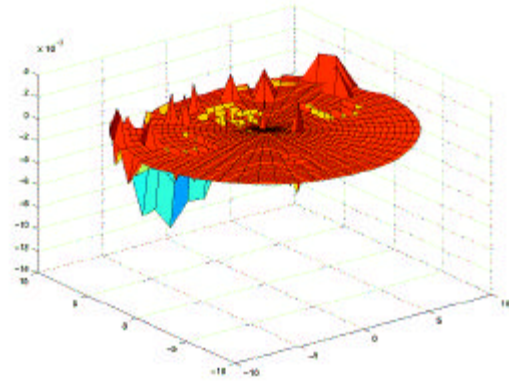


Figure 6: Error of electric field (Real) for circular domain

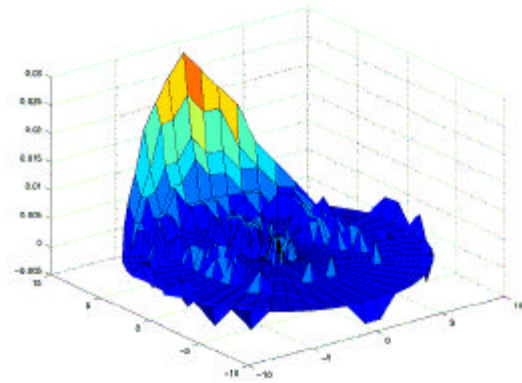


Figure 7: Error of electric field (Imaginary) for circular domain

5. RECONSTRUCTION ALGORITHM

5.1 Inverse problem

In forward part of our method, the scattered field E_s is calculated by assuming the function f is known. This is achieved by first solving E_1 in (12) and then calculating E_s in (15). In the inverse part, E_s is known then f is determined. To emphasise the dependency of E_1 and E_s on f , we rewrite (12) and (15) as:

$$E_1(\mathbf{r}, \bar{\mathbf{r}}; f) = E_{i1}(\mathbf{r}, \bar{\mathbf{r}}) + I \int_{\Omega_1} G_1^1(\mathbf{r}, \mathbf{r}') f(\mathbf{r}') E_1(\mathbf{r}', \bar{\mathbf{r}}; f) d\Omega' \quad (18)$$

$$E_s(\bar{\mathbf{r}}; f) = I \int_{\Omega_1} G_3^1(\bar{\mathbf{r}}, \mathbf{r}') f(\mathbf{r}') E_1(\mathbf{r}', \bar{\mathbf{r}}; f) d\Omega' \quad (19)$$

We can see that the scattered field E_s is nonlinearly related to f because the electric field E_1 is a function of f . A popular method useful for the above problem is the so-called "distorted Born approximation (DBA)" [11,12].

5.2 Distorted Born Approximation

Assume that we obtain a known profile f_e which is closed to the function f . In the spirit of the DBA, we can write:

$$E_s(\bar{r}; f) \approx I \int_{\Omega_1} G_3^1(\bar{r}, r') f(r') E_1(r', \bar{r}; f_e) d\Omega' \quad (20)$$

where $E_1(r, \bar{r}; f_e)$ is the electric field solved from equation (18) with the profile f_e . The profile f is now linearly related to E_s . In the next section, we derive an iterative procedure to reconstruct the actual profile f_0 within the DBA framework. However, it should be mentioned that DBA is not a necessary condition for our method. In [8], we provide a full account of the method without DBA.

5.3 Iterative Procedure

From (20), we define an error functional $U(r; f)$:

$$U(r; f) = E_{s0}(r) - E_s(r; f) \quad (21)$$

where

$$E_{s0}(\bar{r}) \approx I \int_{\Omega_1} G_3^1(\bar{r}, r') f_0(r') E_1(r', \bar{r}; f_0) d\Omega' \quad (22)$$

It is a quantity that we can measure. We have:

$$U(r; f) = E_{s0}(\bar{r}) - I \int_{\Omega_1} G_3^1(\bar{r}, r') f(r') E_1(r', \bar{r}; f_e) d\Omega' \quad (23)$$

If the measurements are taken at L different positions, we want to find such an f that minimises

$$\sum_{l=1}^L |U(\bar{r}_l; f)|^2 \quad (24)$$

subjected to the integral equation (18). Assume that we know an estimate of the function f to be f_m . We want to find a better estimate by adding a small increment δf_m to f_m .

We start with the first order Taylor series expansion:

$$|U(\bar{r}; f + df)|^2 \approx |U(\bar{r}; f)|^2 + 2\text{Re}[U^*(\bar{r}; f) dU(\bar{r}; f)] \quad (25)$$

where $dU(\bar{r}; f)$ can easily be obtain using (23):

$$dU(\bar{r}; f) = I \int_{\Omega_1} G_3^1(\bar{r}, r') df(r) E_1(r', \bar{r}) d\Omega' \quad (26)$$

The variation in $f(r)$ is given by:

$$df(r) = f_a(r) da + f_r(r) dr(j) \quad (27)$$

Note that as $\alpha \rightarrow \infty$ (there is no mushy zone), $f_r(r) \rightarrow d[r - r(j)]$, $f_a(r) \rightarrow 0$. Under this condition, double integral in (26) is reduced to single integral. For a smooth curve, $r(j)$ can be approximated by a truncated Fourier series of $2N+1$ terms:

$$r(j) = \sum_{n=0}^N A(n) \cos(nj) + \sum_{n=1}^N B(n) \sin(nj) \quad (28)$$

An iterative procedure is used to update parameters $A(n)$, $B(n)$ and a until a true solution is achieved. Equation (22) can be written as:

$$|U(\bar{r}; f + df)|^2 \approx |U(\bar{r}; f)|^2 + daD(\bar{r}) + \sum_{n=0}^N dA(n)C(n; \bar{r}) + \sum_{n=1}^N dB(n)S(n; \bar{r}) \quad (29)$$

$$D(n; \bar{r}) = -2\text{Re}\left\{U^*(\bar{r}; f) I \int_{\Omega_1} \left[G_3^1(\bar{r}, r') f_a(r') \right] E_1(r', \bar{r}) d\Omega' \right\} \quad (30)$$

$$C(n; \bar{r}) = -2\text{Re}\left\{U^*(\bar{r}; f) I \int_{\Omega_1} \left[G_3^1(\bar{r}, r') f_r(r') E_1(r', \bar{r}) \cos(nj') \right] d\Omega' \right\} \quad (31)$$

The expression for $S(n; \bar{r})$ is the same as that for $C(n; \bar{r})$ with $\sin(n\phi)$ replacing $\cos(n\phi)$. In matrix form, equation (29) is:

$$|U(\bar{r}; f + df)|^2 \approx |U(\bar{r}; f)|^2 + \mathbf{p}^T(\bar{r}) d\mathbf{q} \quad (32)$$

where

$$\mathbf{p}(\bar{r}) = \text{vec}\{D(\bar{r}), C(n; \bar{r}), S(n; \bar{r})\} \quad (33)$$

$$\mathbf{q} = \text{vec}\{a, A(n), B(n)\} \quad (34)$$

For L measurements, (32) becomes:

$$\mathbf{e} = \mathbf{u} + \mathbf{P}d\mathbf{q} \quad (35)$$

where

$$\mathbf{e} = \text{vec}\{U(\bar{r}_1; f + df), \dots, U(\bar{r}_L; f + df)\} \quad (36)$$

$$\mathbf{u} = \text{vec}\{U(\bar{r}_1; f), \dots, U(\bar{r}_L; f)\} \quad (37)$$

$$\mathbf{P} = \text{vec}\{\mathbf{p}^T(\bar{\mathbf{r}}_1), \dots, \mathbf{p}^T(\bar{\mathbf{r}}_L)\} \quad (38)$$

Let $f_m(\mathbf{r})$ be the m th estimate whose parameters are $A_m(n)$, $B_m(n)$ and \mathbf{a}_m . Then this estimate can be used as the function f_e ($f_e(\mathbf{r})=f_m(\mathbf{r})$) for the distorted Born approximation. It is then updated by finding an increment δf_m such that $\sum_{i=1}^L |U(\bar{\mathbf{r}}_i; f_m + \delta f_m)|^2$ is minimised. This can be done via the increment $\delta \mathbf{q}_m$:

$$d\mathbf{q}_m = \arg \min_{\mathbf{x}} \|\mathbf{u}_m + \mathbf{P}_m \mathbf{x}\| \quad (39)$$

In general it is not possible to find $\delta \mathbf{q}_m$ by minimising the above norm. This is due to the ill-conditioning of the matrix \mathbf{P} . When noise exists in measurements, the increment $\delta \mathbf{q}_m$ may be very large. Regularisation can reduce this effect. Many different techniques such as singular value decomposition, total least squares, constrained optimisation can be used [13].

6. FAST COMPUTATION

Reconstruction of the profile $f(\mathbf{r})$ requires a lot of 2-D numerical integration, which is time consuming. Due to the complex geometry in our problem, the Green functions are tedious and computationally demanding. In this section, we derive a procedure to speed up the computation considerably. The idea is based on the Gaussian quadrature [14] formula. Adaptive Gaussian quadrature subdivides the intervals $[0, 2\pi]$ and $[0, r_1]$ and applies Gauss rule to estimate the integral over each subinterval.

Let us consider the following integral:

$$\int_{j_1}^{j_2} \int_a^b G_1^1(\mathbf{r}, \mathbf{r}') f(\mathbf{r}') c_1(\mathbf{r}') d\Omega' \quad (40)$$

where $\chi(\mathbf{r})$ is one of the basis function for the moments method, $[j_1, j_2] \in [0, 2\pi]$, $[a, b] \in [0, r_1]$. In our iterative procedure, the profile changes after each iteration and hence the integral (32) has to be evaluated again and again. We will show that there is no need to do so. Consider the profile $f(\mathbf{r})$ as a weighting function, which is nonnegative and integrable on the specified region. For Gaussian quadrature, we can write (32) as:

$$I \approx \frac{j_2 - j_1}{2} \frac{b - a}{2} \sum_{i=1}^K \sum_{j=1}^M c_i d_j(j_i) G_1^1 \left(r_j, \frac{(b-a)r_j + b + a}{2}, \frac{(j_2 - j_1)j_i + j_2 + j_1}{2} \right) c \left(\frac{(b-a)r_j + b + a}{2}, \frac{(j_2 - j_1)j_i + j_2 + j_1}{2} \right) \quad (41)$$

where K and M are integers and the weights c_i , $d_j(j_i)$ is related to the nodes (r_j, j_i) by Vandermonde matrices [8]:

$$\begin{bmatrix} c_1 \\ \vdots \\ c_K \end{bmatrix} = \begin{bmatrix} 1 & \dots & 1 \\ \vdots & \ddots & \vdots \\ j_1^K & \dots & j_K^K \end{bmatrix}^{-1} \mathbf{h} \quad (42)$$

$$\begin{bmatrix} d_1(j) \\ \vdots \\ d_M(j) \end{bmatrix} = \begin{bmatrix} 1 & \dots & 1 \\ \vdots & \ddots & \vdots \\ r_1^M & \dots & r_M^M \end{bmatrix}^{-1} \mathbf{f} \quad (43)$$

where

$$\mathbf{h} = \text{vec}\{j_2 - j_1, \dots, (j_2^K - j_1^K) / K\} \quad (44)$$

$$\mathbf{f} = \text{vec}\left\{ \int_a^b f(r'j) r' dr', \dots, \int_a^b f(r'j) r'^M r' dr' \right\} \quad (45)$$

The nodes r_j and j_i are roots of the M th and K th degree Legendre polynomials respectively. They are extensively tabulated [15], so it is not necessary to perform roots finding. All the quantities can be pre-computed off-line except for the vector \mathbf{f} which is computationally very fast. Every time the profile $f(\mathbf{r})$ is updated, we only need to evaluate \mathbf{f} .

7. SIMULATION

The parameters used in the simulation are:

Permeability	m	$4\pi \times 10^{-7}$ (H/m)
Conductivity of solidified metal	s_s	2×10^6 (mhos/m)
Conductivity of Molten metal	s_l	1×10^6 (mhos/m)
Conductivity of pipe	s_p	1×10^5 (mhos/m)
Frequency	w	$2\pi \times 10^2$ (rad/s)
Inner radius of pipe	r_1	15×10^{-3} (m)
Outer radius of pipe	r_2	16×10^{-3} (m)
Radial distance of Line source	r_3	25×10^{-3} (m)

Table 1. Values of parameters.

Table 2 shows the estimates of parameters after 15 iterations.

Var	True	Initial	2nd	4th	6th
a	5.000	1.000	1.461	2.117	2.610
A_0	10.200	8.000	9.983	10.142	10.172
A_1	3.600	0.000	3.284	3.604	3.658
A_2	-0.850	0.000	-0.428	-0.756	-0.822
A_3	1.700	0.000	1.905	1.781	1.750
B_1	1.100	0.000	0.964	1.088	1.112
B_2	-1.300	0.000	-1.116	-1.269	-1.301
B_3	0.900	0.000	0.779	0.833	0.902

Var	8 th	10th	12th	14th	15th
a	3.557	4.289	4.700	4.883	4.929
A_0	10.189	10.196	10.198	10.199	10.200
A_1	3.629	3.613	3.606	3.602	3.601
A_2	-0.844	-0.848	-0.849	-0.850	-0.850
A_3	1.720	1.708	1.703	1.701	1.701
B_1	1.107	1.103	1.102	1.101	1.100
B_2	-1.303	-1.302	-1.301	-1.300	-1.300
B_3	0.902	0.901	0.900	0.900	0.900

Table 2: Convergence of parameters

It can be seen that that convergence is quite fast. Figure 8 and 9 show the shape function $r(j)$ after 3 iterations.

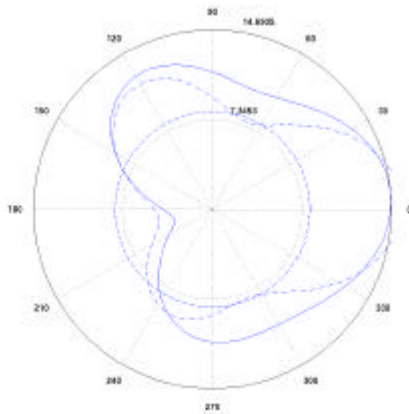


Figure 8: True shape (—), the intial (--) and the first (— · —) estimates

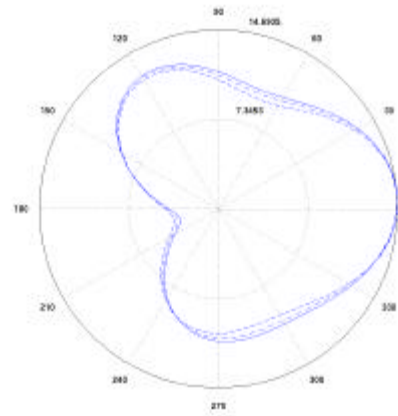


Figure 9: True shape (—), the 2nd (--) and the 3rd (— · —) estimates

Define the Relative Mean Square Error (RMSE) of the parameters of the shape $r(j)$ at the k th iteration as:

$$\sqrt{\frac{\sum_{n=0}^N (A_k(n) - A_0(n))^2 + \sum_{n=1}^N (B_k(n) - B_0(n))^2}{\sum_{n=0}^N A_0^2(n) + \sum_{n=1}^N B_0^2(n)}}$$

It can be seen in Figure 10 that the RMSE for $r(j)$ rapidly decreases after each successive iteration. The parameter a also converges quite well to the actual value. The conductivity profile can now be reconstructed from these parameters.

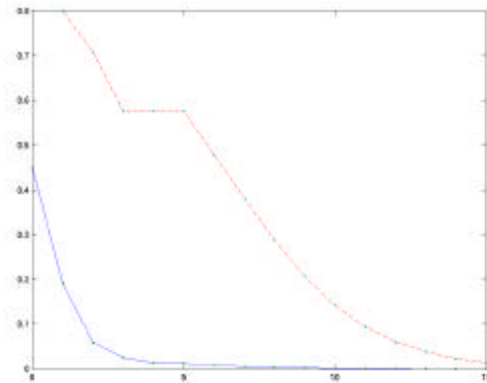


Figure 10: Relative error vs. No. of iterations (RMSE of $\rho(\phi)$ (—) and α (--))

8. CONCLUSION

The paper has presented an imaging technique for reconstructing the shape and thickness of solidification using eddy currents. The eddy currents are characterised by differential equations. Using the superposition theorem and Green functions, we have converted these equations into a set of integral equations which yield an indirect relationship between the conductivity distribution and the observable impedance. Based on this relationship an iterative reconstruction algorithm has been derived. At each step of iteration, the electric field inside the pipe is solved numerically by moments method with Fourier series and polynomial approximation. Gaussian quadrature with the profile as a weighting function speeds up the computation considerably. Simulation results show that the algorithm does really converge to the true image. Further issues such as noise, convergent property of the iterative algorithm, dependency of parameters on temperature remain to be investigated.

REFERENCES

- [1] J. S. Pitsillos, Y. L. Yeow, and N. B. Gray, "Flow control in a subcooled tube: an experiment investigation of the effect of crust formation.", *International Journal of Heat and Mass Transfer.*, vol.40, no. 18, pp.4337-4343, 1997.
- [2] J. P. Wallace, and D. C. Kunerth, "Eddy current response to metallic solidification in one dimension", *Metallurgical Transaction B*, vol. 11B. pp.267-271, 1980.
- [3] D. C. Kunerth, and J. P. Wallace, "Eddy current study of solidification in lead and lead 20 pct tin", *Metallurgical Transaction B*, vol. 11B. pp.273-283, 1980.
- [4] D. P. Cook, S. Nishioka and J. W. Evans, "A Three-Dimensional Mathematical Model of Electromagnetic Casting and Testing against a Physical Model: Part II. Results from a Physical Model and Testing of the Mathematical Model", *Metallurgical and Materials Transactions B*, vol. 26B, pp.1271-1279, Dec. 1995.
- [5] J. A. Stratton, *Electromagnetic Theory*, McGraw-Hill, New York and London, 1941.
- [6] A. B. Crowley and J. R. Ockendon, "Modelling mushy regions", *Applied Scientific Research*, vol. 44, pp.1-7, 1987.
- [7] C. Beckerman, L. A. Bertram, S. J. Pien and R. E. Smelser, *Micro/Macro Scale Phenomena in Solidification*, HTD-Vol. 218/AMD-Vol. 139, ASME, 1992.
- [8] H. P. Minh, Y. Hua and N. B. Gray, "Imaging the solidification of molten metal by eddy current", *Ph. D Annual Report, full version*, Melbourne University, Dec 1998.
- [9] R. F. Harrington, "Matrix methods for field problems", *Proc. IEEE*, vol. 55, pp.136-149, Feb. 1967.
- [10] R. F. Harrington, *Field Computation by Moments Method*, MacMillian, New York, 1968.
- [11] A. J. Devaney, "Inversion Procedure for Inverse Scattering within the Distorted-Wave Born Approximation", *Physical Review Letters*, vol. 51, pp.237-240, July 1983.
- [12] W. C. Chew and Q. H. Liu, "Inversion of Induction Tool Measurements Using the Distorted Born Iterative Method and CG-FFHT", *IEEE Trans. Geoscience and Remote Sensing*, Vol. 32, pp.878-884, July 1994.
- [13] G. H. Golub and C. F. V. Loan, *Matrix Computation*, North Oxford Academic, Oxford, 1983.
- [14] K. E. Atkinson, *An Introduction to Numerical Analysis*, Wiley, Singapore, 1988.
- [15] M. Abramowitz and I. A. Stegun, *Handbook of Mathematical Functions, with Formulas, Graphs, and Mathematical Tables*, Dover Publications, Inc., New York, 1970.